Optical diagnostics of femtosecond laser plasmas

LI Yutong (李玉同)[1,2], ZHANG Jie (张 杰)[1], CHEN Liming (陈黎明)[1,2], XIA Jiangfan (夏江帆)[1], TENG Hao (腾 浩)[1], ZHAO Lizeng (赵理曾)[1], LIN Jingquan (林景全)[1], LI Yingjun (李英骏)[1], WEI Zhiyi (魏志义)[1], WANG Long (王 龙)[1] & JIANG Wenmian (江文勉)[2]

1. Institute of Physics, Chinese Academy of Sciences, Beijing 100080, China;
2. Research Center of Laser Fusion, China Academy of Engineering Physics, Mianyang 621900, China
Correspondence should be addressed to Zhang Jie (email: jzhang@aphys.iphy.ac.cn)

Received June 8, 2000

Abstract Optical diagnostics of evolution of plasmas produced by ultrashort laser pulses is carried out using a femtosecond probing beam. The time sequence of plasma shadowgrams and interferograms are obtained. The filamentation instability in high-density region induces the local density modification. Large-scale toroidal magnetic fields confine plasma expansion in the transverse direction, resulting in the formation of a plasma jet. The plasma expansion along the target normal direction is found to scale as $t^{1/2}$.

Keywords: **femtosecond laser plasma, optical diagnostic, electron density gradient.**

Laser probing technique, which does not perturb the measured medium, is a novel method to diagnose dense plasmas. Much information can be obtained by carefully analyzing the results from the probing beam, such as intensity, phase, polarization and angular scattering. The laser probing technique is extensively used in Inertial Confinement Fusion (ICF), Z-pinch and X-ray laser plasma diagnostics. For example, shadowgraphy, schlieren techniques and moire deflectometry based on the reflection of probing beams in plasmas are concerned with the electron density gradients. Interferometry is a primary experimental technique for measuring the plasma refractive properties which are related to the electron density.

Many important processes in plasmas, such as density steepening by ponderomotive forces, filamentation of laser pulses, the plasma channel formation in the context of fast ignition, energy absorption and other phenomena, have been studied with the help of laser interferometry. The electron density gradient scale is a basic parameter for theoretical simulations. Accurate measurement of electron density distribution is an important task for experimental researchers.

Because of the expansion and recombination of laser plasma, it is difficult to determinate the electron density accurately using a long pulse (nanosecond) laser probing beam. In this respect, subpicosecond laser pulses can effectively freeze the motion of plasmas. Use of short pulses in optical diagnostics is advantageous compared with the use of a long pulse laser probing beam. In this paper, temporal evolution of plasmas produced by ultrashort laser pulses was observed using femtosecond laser probing techniques. Various shadowgrams and interferograms at different time show plasma jet formation in the interaction.

1 Experiments

The schematic setup of experiments is shown in fig. 1. A small percent of the 800-nm laser

light was split from the main beam; frequency doubled by a BBO crystal to 400-nm, and probed the plasma along the target surface. The plasma was imaged by a telescope with 14 × magnification on a 16 bit, 1 152 × 1 242 pixels CCD camera. A modified Nomarski interferometer[1] was used to measure the electron density. Two plasma images shifted laterally from one another in the same plane by a 2° wollaston prism with a 10 mm × 10 mm cross section made of calcite. Interference between these two images was achieved by a polarizer and an analyzer with certain orientation. Two Glan-Taylor prisms (12 mm × 12 mm aperture) with extinction ratio better than 10^{-5} were used. The configuration acted as a polarimeter to measure the self-generated magnetic fields in plasmas when the Wallaston prism was removed. Interferograms and shadowgrams were obtained by adjusting the optical path between the main laser beam and the probing beam. The plasma image disappeared on the detector when the main beam and the probing beam were synchronized exactly. This time was set to be timing zero reference.

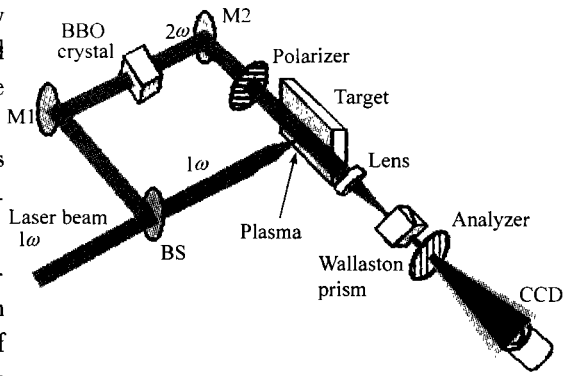

Fig. 1. Experimental setup for shadowgraphy, and interferometry, where BS is a beamsplitter, and M represents reflect mirror.

The experiments were performed using pulses of 5 mJ and 150 fs duration at 800 nm with 10 Hz frequency produced by a Ti:sapphire laser at the Institute of Physics. The beam was focused on 3 μm thick aluminum layer coated on glass substrate at about intensity of 5×10^{15} W/cm^2. The incident angle was set to be 0° for all experiments presented here. The target moved 1 mm after every shot so that the laser pulses interacted with a fresh target surface. Complex application of neutral and interference filters with narrow bandwidth singled out the 400-nm probe beam from other background emission. The pixel size of the CCD camera is 25 μm, which gives a pixel-limited spatial resolution ~ 2 μm. The time resolution is determined by duration of probe beam, which is about 150 fs.

2 Results and discussion

The shape and size of the plasma measured are obtained by shadowgraphy technique, which maps the dense region of the plasma. The deviation angle of a light ray passing through plasma is written as

$$\alpha = \int \nabla_{\perp} \eta \mathrm{d}l, \tag{1}$$

where $\nabla_{\perp} \eta$ is the transverse refractive index gradient. It varies in space generally. Adjacent rays are deviated by different amounts, resulting in a change of the intensity distribution at the detector plane. Fig. 2 shows the plasma shadowgram taken 13 ps after the main laser beam. From the shadowgram, the gradual variation of the intensity in the target normal direction can be seen since the density gradient reduces along the normal direction.

We first estimate the upper limit of the electron density accessible for a 400 nm probing beam in our optical systems before the discussion. It is well known that the values measured are far lower than that of the critical density since the incident probing beams are absorbed, reflected, or deflected by the plasma. One of the major limitations is the acceptance angle of the imag-

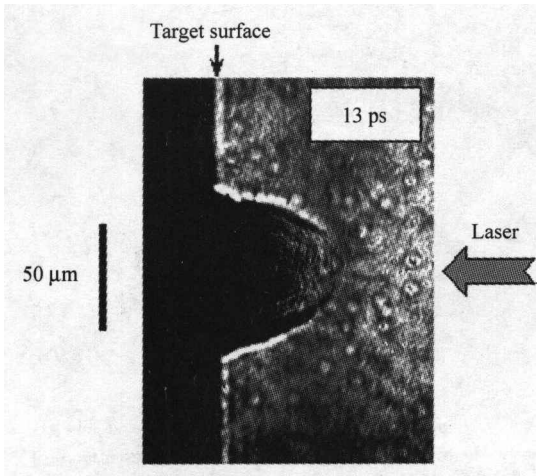

Fig. 2. A typical shadowgram for 13 ps of Al target.

ing lens, i.e. $1/2F$, where F is the f-number of the lens. An approximate expression of the deviation angle of the probing beam through a plasma, from eq. (1), is $\alpha = \frac{n_e}{2n_c}\frac{l}{L}$, where L is the plasma length, l is the density gradient scale-length, n_e and n_c are the density and critical density respectively. The acceptance angle 0.15 rad of the imaging lens gives the detectable maximum density 2×10^{20} cm^{-3} for 400 nm probing beam when L and l are set to be 100 and 10 μm respectively. This value is confirmed by the following experimental results.

The presence of a plasma into the probing beam produces a phase shift with respect to the reference beam. The number of fringe shifts N is given by

$$N = \int_0^L \frac{\Delta\eta}{\lambda} dx \approx \frac{L}{2\lambda}\frac{n_e}{n_c}, \tag{2}$$

where λ is the wavelength of the probing beam, L is the plasma length along the path of the probing beam, and η is the index of refraction of the plasma, which is written as $\eta = (1 - n_e/n_c)^{1/2}$, where n_c is the critical electron density for the probing laser beam.

The distribution of electron density can be obtained using the famous Abel inversion under the assumption of axial-symmetry. However, the interferograms recorded on the CCD camera were non-symmetry at later time (see fig. 3). Several methods of Abel inversion were used in order to estimate the density distribution. First, the axis of Abel inversion was set at the plasma center; the density maps of the first quadrant and the second quadrant were obtained by abelizing the upper and lower parts of the interferogram studied respectively. Then we had the overall density distribution after combining the two quadrants. We differently set the axis of Abel inversion on the side of plasma, and imagined the practical plasma located in the first quadrant of a big imaginary plasma region in the last method. Compared with the results obtained by these methods, we found that the last one gave lower density values, though the overall density map could be acquired. Here a set of interferograms at three different moments and the corresponding density maps obtained by Abel inversion using the first method are shown in fig. 3, where the density is in 10^{19} cm^{-3}. To avoid the confusion introduced by the Abel inversion, the following analysis is based on the interferograms and the phase shift distributions mainly. Some important features can be seen from the interferograms. (i) Fringes are not clear at early time, and are obvious at later time after the femtosecond pulse interaction. This is because the plasma density gradient relaxes at later time, leading to small refraction of the probing beam. (ii) The interferograms are not axial-symmetric and the density collapses. A jet of plasma forms in the longitudinal direction. (iii) Some small-scale fringes appear in the interferograms. Although the density values were different slightly, the shapes of density distributions obtained by all four Abel inversion methods mentioned above possessed similar characteristics with the interferograms. The first feature is understood easily. We will discuss the last two features in the following.

Small-scale density modifications are related with instabilities occurring in the plasma. One

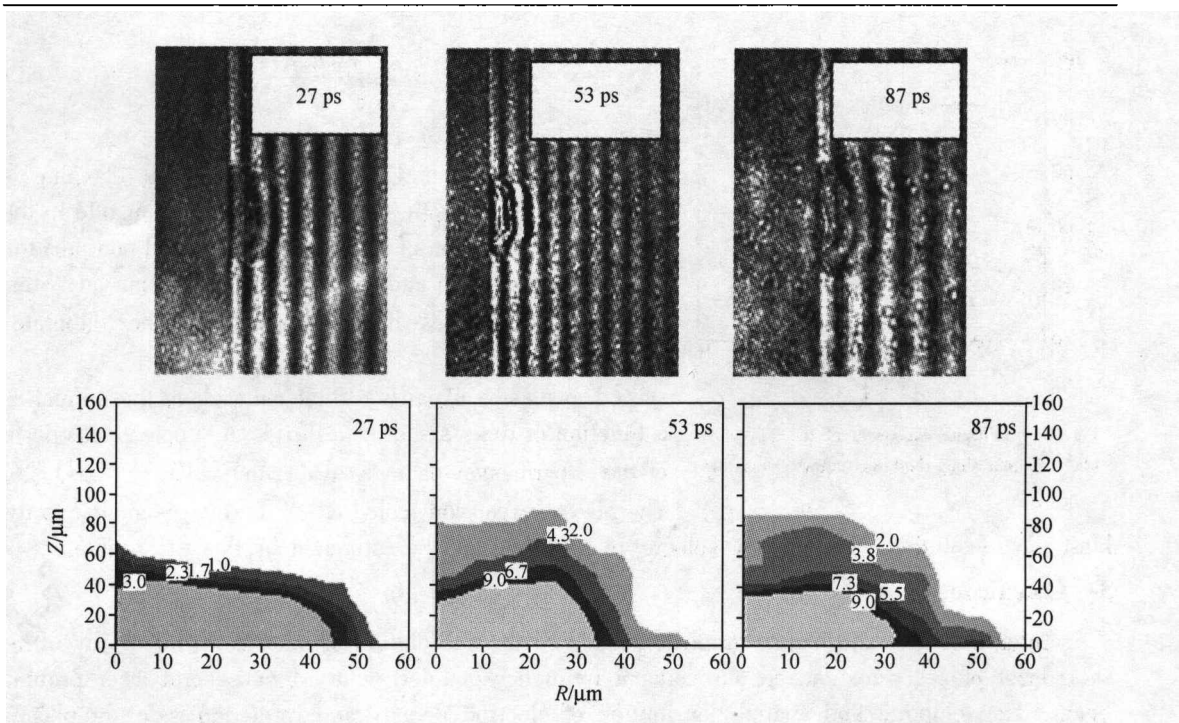

Fig. 3. A series of interferograms and density distribution at different time (density in 10^{19} cm^{-3}).

of the important instabilities is the filamentation instability, in which the laser beam breaks up into higher intensity spots. The filamentation threshold intensity is given by[2]

$$I_{\mathrm{th}} = 2 \times 10^{15} L_{\mu}^{-1} \lambda_{\mu}^{-1} T_{\mathrm{keV}} \frac{n_{\mathrm{c}}}{n_{\mathrm{e}}}, \tag{3}$$

where L_{μ} is the plasma length in micron, λ_{μ} is the laser wavelength in micron, and T_{keV} is the electron temperature in keV. The threshold value is high in the outer region of the plasma because of the low density and the high temperature there. The case is inverse in dense plasma region. Taking $L \sim 100$ μm, $\lambda \sim 0.8$ μm, $T \sim 5$ keV[3], the threshold intensity $I_{\mathrm{th}} \sim 1.25 \times 10^{16}$ W·cm^{-2} for $n_{\mathrm{e}}/n_{\mathrm{c}} = 0.01$. However, the threshold intensity reduces to 1.25×10^{15} W·cm^{-2} for $n_{\mathrm{e}}/n_{\mathrm{c}} = 0.1$. Under our experimental conditions (5×10^{15} W·cm^{-2}), the filamentation instability can take place in higher density regions, but it cannot develop in lower regions. The filamentation of laser pulse increases the local intensity and the temperature, which affect the local density distribution. Since the filamentation takes place during the pulse duration and in higher density region where the refraction effect is serious so that only very low region is accessible for the probing beam, the fringes at earlier time are regular, which cannot detect the density modification in dense region induced by filamentation. However, the after-effect of filamentation at later time shows on in the interferograms. Filamentation cannot explain the density collapse and the formation of the plasma jet.

Theoretical and experimental studies show that very strong quasistatic magnetic fields are generated in the interaction of laser pulses with plasmas[4]. The large-scale toroidal magnetic fields excited by the mechanism of nonlinear of density gradient and temperature are explored extensively[5, 6]. The strong magnetic fields can pinch plasma, and change the plasma expansion. The ratio of magnetic field pressure to thermal pressure is

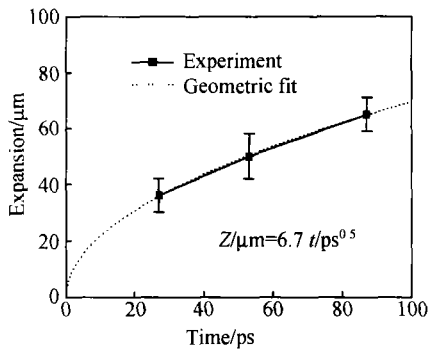

Fig. 4. Plasma expansion of the 2.0×10^{19} cm^{-3} contour along the target normal versus time.

$$\beta = \frac{8\pi n_e kT}{B^2}, \tag{4}$$

where k is the Boltzmann constant. When we take $n_e = 2 \times 10^{19}$ cm^{-3}, $T = 5$ keV, $B = 2$ MG, the β value is about 1, i.e. magnetic field plays an important role in the hydrodynamic motion of the plasma. The field confines the transverse expansion and formation of the plasma jet. Similar phenomenon has been observed in other laboratories[7, 8].

The plasma expansion dimension along the normal as a function of time is shown in fig. 4. A simple geometric fit of the experimental data gives $Z(\mu m) = 10.3[t(ps)]^{0.5}$. The plasma expansion scaled as $t^{1/2}$, which is similar to the blast wave evolution. The moving velocity of a plasma can be estimated by this fit formula.

3 Conclusions

Interferometric and shadowgraphic measurements of evolution of plasmas produced by ultrashort laser pulses were carried out using a frequency-doubled (2ω) femtosecond laser probing beam. The temporal and spatial distribution of electron density and refraction index of plasma were obtained after abelizing the time sequence of interferograms. The filamentation instability and other instabilities in high-density region induced the local density modification. Large-scale toroidal magnetic fields confined plasma expansion in the transverse direction, resulting in the formation of plasma jet. The plasma expansion along the target normal scaled as $t^{1/2}$.

Acknowledgements The authors wish to thank the laser staff at the Laboratory of Optical Physics, Institute of Physics, Chinese Academy of Sciences. This work was supported by the National Natural Science Foundation of China (Grant Nos. 19854001 & 19825110), the National High-Tech ICF Committee, the Laboratory for Laser Fusion of China Academy of Engineering Physics, and the Pre-research Foundation of CAEP.

References

1. Benattar, R., Popovics, C., Sigel, R., Polarized light interferometer for laser fusion studies, Rev. Sci. Instrum., 1979, 50(12): 1583.
2. Young, P. E., Hammer, J. H., Wilks, S. C. et al., Laser beam propagation and channel formation in underdense plasmas, Phys. Plasmas, 1995, 2(7): 2825.
3. Zhang, P., He, J.T., Chen, D.B. et al., Effects of a prepulse on γ-ray radiation produced by a femtosecond laser with only 5 mJ energy, Phys. Rev. E., 1998, 57: R3746.
4. Stamper, J. A., Review on spontaneous magnetic fields in laser-produced plasmas: phenomena and measurements, Laser and Particle Beams, 1991, 9(4): 841.
5. Stamper, J. A., McLean, E. A., Ripin, B. H., Studies of spontaneous magnetic fields in laser-produced plasmas by Faraday rotation, Phys. Rev. Lett., 1978, 40(18): 1177.
6. Raven, A., Willi, O., Rumsby, P. T., Megagauss magnetic field profiles in laser-produced plasmas, Phys. Rev. Lett., 1978, 41(8): 554.
7. Burgess, M. D. J., Luther-Davis, B., Nugent, K. A., An experimental study of magnetic fields in plasmas created by high intensity one micron laser radiation, Phys. Fluids, 1985, 28(7): 2286.
8. Borghesi, M., Mackinnon, A. J., Bell, A. R. et al., Megagauss magnetic field generation and plasma jet formation on solid targets irradiated by an ultraintense picosecond laser pulse, Phys. Rev. Lett., 1998, 81(1): 112.